A-site ordered perovskite $CaCu_3Cu_2Ir_2O_{12-\delta}$ with square-planar and octahedral coordinated Cu ions*

Qing Zhao(赵庆)[1,2], Yun-Yu Yin(殷云宇)[2], Jian-Hong Dai(戴建洪)[2], Xi Shen(沈希)[2], Zhi-Wei Hu(胡志伟)[3], Jun-Ye Yang(杨俊叶)[2], Qing-Tao Wang(王清涛)[1,4,†], Ri-Cheng Yu(禹日成)[2], Xiao-Dong Li(李晓东)[5], and You-Wen Long(龙有文)[2,6,‡]

[1] *College of Physics, Qingdao University, Qingdao* 266071, *China*
[2] *Beijing National Laboratory for Condensed Matter Physics, Institute of Physics, Chinese Academy of Sciences, Beijing* 100190, *China*
[3] *Max-Planck Institute for Chemical Physics of Solids, Nöthnitzer Straße* 40, 01187 *Dresden, Germany*
[4] *Key Laboratory of Photonics Materials and Technology in Universities of Shandong (Qingdao University), Qingdao* 266071, *China*
[5] *Beijing Synchrotron Radiation Facility, Institute of High Energy Physics, Chinese Academy of Sciences, Beijing* 100049, *China*
[6] *Collaborative Innovation Center of Quantum Matter, Beijing* 100190, *China*

(Received 13 October 2015; revised manuscript received 3 November 2015; published online 10 January 2016)

A novel $CaCu_3Cu_2Ir_2O_{12-\delta}$ polycrystalline sample was synthesized at 8 GPa and 1373 K. Rietveld structural analysis shows that this compound crystallizes in an $AA'_3B_4O_{12}$-type *A*-site ordered perovskite structure with space group *Im*-3. X-ray absorption spectra reveal a +2-charge state for both the square-planar and octahedral coordinated Cu ions, and the valence state of Ir is found to be about +5. Although the *A*-site Ca and the *A*′-site Cu^{2+} are 1:3 ordered at fixed atomic positions, the distribution of *B*-site Cu^{2+} and Ir^{5+} is disorderly. As a result, no long-range magnetic ordering is observed at temperatures down to 2 K. Electrical transport and heat capacity measurements demonstrate itinerant electronic behavior. The crystal structure is stable with pressure up to 35.7 GPa at room temperature.

Keywords: high pressure synthesis, *A*-site ordered perovskite, valence state, magnetic property

PACS: 07.35.+k, 61.05.cj, 75.20.–g **DOI:** 10.1088/1674-1056/25/2/020701

1. Introduction

A-site ordered quadruple perovskites with a chemical formula of $AA'_3B_4O_{12}$ have attracted much attention. In this ordered system, both the *A*′ and *B* sites can accommodate transition-metal ions, giving rise to multiple magnetic and electrical interactions such as *A*′–*A*′, *B*–*B*, and *A*′–*B* interactions. As a consequence, a series of intriguing physical properties have been observed in *A*-site ordered perovskite oxides. For example, ferromagnetic phase transitions caused by the *A*′-site Cu^{2+} ions were found in $CaCu_3Ge/Sn_4O_{12}$,[1,2] whereas in $CaCu_3Ti_4O_{12}$ the spin ordering of Cu^{2+} leads to an antiferromagnetic transformation.[3,4] More interesting, temperature/pressure-induced intermetallic charge transfer occurs between the *A*′-site Cu and the *B*-site Fe in $La/BiCu_3Fe_4O_{12}$, resulting in sharp variations in lattice, charge and spin degrees of freedom.[5–7] When the *A*-site La/Bi was replaced by Ca, charge disproportionation instead of charge transfer took place in $CaCu_3Fe_4O_{12}$.[8] Unlike $La/Bi/CaCu_3Fe_4O_{12}$, colossal negative thermal expansion was shown in $SrCu_3Fe_4O_{12}$ in a wide temperature window.[9]

The *A*-site ordered perovskite $AA'_3B_4O_{12}$ usually crystallizes to a cubic crystal structure with space group *Im*-3 as shown in Fig. 1. In this symmetry, the *A* and *A*′ sites are 1:3 ordered to occupy different atomic positions 2*a* (0, 0, 0) and 6*b* (0, 0.5, 0.5), respectively. The *B* site is fixed at 8*c* (0.25, 0.25, 0.25), and the O is located at 24*g* (0, *y*, *z*). Compared to the simple ABO_3 perovskite where the 12-fold coordinated A site is often occupied by alkali metal, alkaline earth, and/or lanthanide cations,[10–12] in the present ordered case, three quarters of the *A*-sites are substituted by a transition metal *A*′ with smaller ionic radius. Therefore, the BO_6 octahedra are heavily tilted (typically, $\angle B$–O–$B \approx 140°$) and the *A*′-site transition metal forms a square-planar $A'O_4$ unit.[13] Since the coordination environment can play an important role for the electronic configuration of transition metals, the *A*-site ordered perovskite provides a unique material system in which to study the effects of coordination on material physical properties. In this paper, we report preparing for the first time the *A*-site ordered perovskite $CaCu_3Cu_2Ir_2O_{12-\delta}$ (CCCIO) with Cu ions occupying the square-planar $A'O_4$ units as well as the octahedral BO_6 polyhedra. Structural and x-ray absorption analyses show that the charge combination is $CaCu_3^{2+}Cu_2^{2+}Ir_2^{5+}O_{12-\delta}$ with $\delta \approx 1$, and the *B*-site Cu^{2+} and Ir^{5+} ions are distributed in a disordered manner. No long-range magnetic ordering is observed at temperatures down to 2 K.

*Project supported by the National Basic Research Program of China (Grant No. 2014CB921500), the Strategic Priority Research Program of the Chinese Academy of Sciences (Grant No. XDB07030300), and the National Natural Science Foundation of China (Grant No. 11574378).

†Corresponding author. E-mail: wangqt@qdu.edu.cn
‡Corresponding author. E-mail: ywlong@iphy.ac.cn

© 2016 Chinese Physical Society and IOP Publishing Ltd

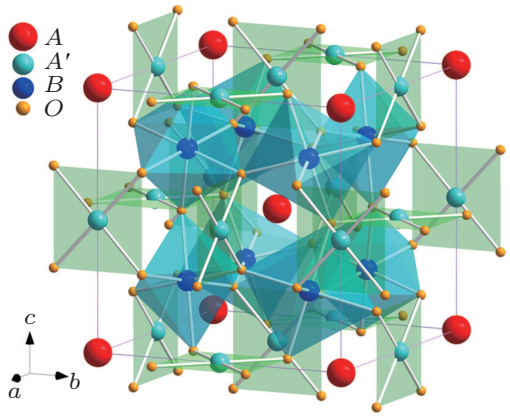


Fig. 1. (color online) Crystal structure of A-site ordered perovskite $AA'_3B_4O_{12}$ with space group Im-3. The A'-site transition metal forms a square-planar $A'O_4$ unit, whereas the B-site transition metal forms an octahedral coordinated BO_6 unit.

2. Experiment

Polycrystalline CCCIO was prepared under high-pressure, high-temperature conditions by using a cubic-anvil-type high-pressure apparatus. Stoichiometric amounts of high-purity ($> 99.9\%$) CaO, CuO, IrO_2 powders were used as starting materials, and excess $KClO_4$ was used as oxygen source. These reactants were mixed thoroughly in an agate mortar. The mixed powders were sealed into a gold capsule with 2.8 mm in diameter and 4.0 mm in length and then treated at 8 GPa and 1373 K for half an hour. When the heating time was finished, the sample was quenched to room temperature, and the pressure was released slowly. The residual KCl in the final product was washed out by deionized water.

The sample purity and crystal structure were examined by powder x-ray diffraction (XRD) using a Rigaku x-ray diffractometer with Cu–K_α radiation (40 kV, 300 mA). The XRD data were collected in the angle range from 10° to 130° with steps of 0.02° and analyzed by the Rietveld refinement using the GSAS program.[14] A Philips CM200 transmission electron microscope (TEM) with a field emission gun operated at 200 keV was used for the select-area electron diffraction (SAED) investigation. The valence states of Cu and Ir were identified by x-ray absorption spectra (XAS) performed at the National Synchrotron Radiation Research Center in Taiwan. The soft XAS at the Cu–L_3 edges were measured with total electron yield at the beamline of BL08B. The hard XAS at the Ir–L_3 edges were measured in the transmission geometry at the BL07A beamline.

Magnetic susceptibility and magnetization were measured using a Quantum Design superconducting quantum interference device magnetometer. The temperature dependence of the magnetic susceptibility was measured at 0.1 T over a range from 2 K to 300 K. The field dependence of the magnetization was measured at several temperatures and under fields from −7 T to 7 T. Temperature dependence of resistivity and specific heat were measured by using a Quantum Design physical property measurement system.

High-pressure synchrotron x-ray diffraction (SXRD) at room temperature was performed at Beijing Synchrotron Radiation Facility. The wavelength used for this experiment was $\lambda = 0.6199$ Å. The powder sample was pressurized using a diamond anvil cell (DAC) with a pair of 300-μm culet. Silicone oil was used as pressure transmitting medium and the pressures were calibrated on the basis of the ruby fluorescence method.[15] The SXRD data were analyzed using the Rietveld refinement program GSAS.

3. Results and discussion

Figure 2 shows the powder XRD pattern measured at room temperature as well as the Rietveld refinement results of CCCIO. The XRD pattern can be well fitted based on the A-site ordered perovskite structure model with space group Im-3. This means that the B-site Cu and Ir ions are arranged randomly over the available octahedral sites. Furthermore, when the SAED is performed, one can find no evidence of B-site ordering. As an example, the inset of Fig. 2 shows the SAED pattern obtained along the $[1\bar{1}0]$ zone axis. The absence of diffraction spots with $h+k+l$ = odd confirms the B-site disorder.[16,17] Therefore, the present CCCIO crystallizes in the same crystal structure as that of $CaCu_3Cr_2Ru_2O_{12}$, wherein the B-site Cr^{3+} and Ru^{5+} are also disordered.[18,19] The refined structural parameters of CCCIO are listed in Table 1. The lattice parameter of CCCIO (7.4481 Å) is slightly less than that of $CaCu_3Ir_4O_{12}$ (7.4738 Å) due to partial substitution of Ir by Cu ions at the B site.[20] According to the A'-site Cu–O bond lengths, the calculated bond valence sum (BVS) of Cu is 1.92, indicating a Cu^{2+} state in this square-planar site.

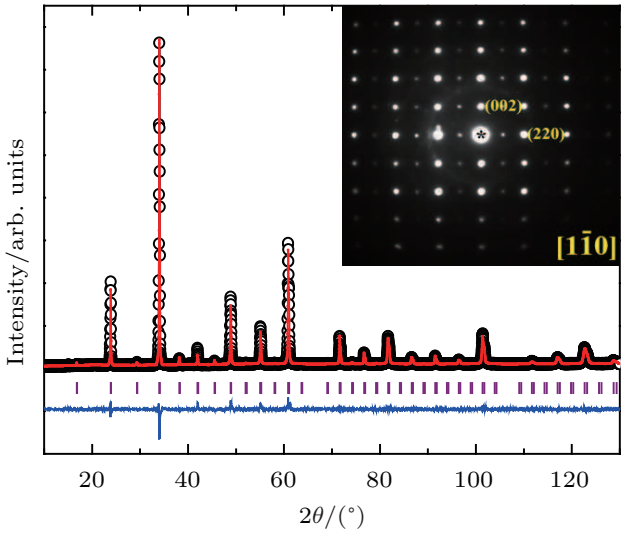


Fig. 2. (color online) XRD pattern and the Rietveld refinement profile of $CaCu_3Cu_2Ir_2O_{12-\delta}$. The observed (circles), calculated (red line), and difference (blue line) patterns are shown. The ticks show the positions of the Bragg reflections with space group Im-3. The inset shows the SAED image along the $[1\bar{1}0]$ zone axis.

Table 1. Refined structure parameters of $CaCu_3Cu_2Ir_2O_{12-\delta}$ at room temperature. Space group: *Im*-3; Atomic sites: Ca 2*a* (0, 0, 0), Cu 6*b* (0, 0.5, 0.5), Cu/Ir 8*c* (0.25, 0.25, 0.25), O 24*g* (0, *y*, *z*).

Parameter	CCCIO
a/Å	7.44817(4)
O_y	0.181
O_z	0.307
U_{iso} (Ca)/(100 × Å^2)	0.04(6)
U_{iso} (Cu)/(100 × Å^2)	2.14(5)
U_{iso} (Cu/Ir)/(100 × Å^2)	0.5(2)
U_{iso} (O)/(100 × Å^2)	0.04(1)
Ca–O/(×12 Å)	2.654(4)
Cu–O/(×4 Å)	1.970(7)
(×4) (Å)	2.777(1)
(×4) (Å)	3.297(5)
Cu/Ir–O/(×6 Å)	1.977(7)
∠O–Cu–O/(°)	93.6(7)
∠O–Cu/Ir–O/(°)	90.7(5)
∠Cu/Ir–O–Cu/Ir/(°)	140.6(1)
∠Cu–O–Cu/Ir/(°)	109.5(3)
R_{wp}/%	7.15
R_p/%	5.22

X-ray absorption spectrum at the transition-metal L_3 edge is element-specific and sensitive to the valence state as well as the local environment of the transition metal. The valence states of Cu and Ir in our CCCIO are therefore determined by XAS method. Figure 3(a) shows the Cu–L_3 XAS of CCCIO together with $Ca_{0.83}Cu^{2.34+}O_2$ and $CaCu_3^{2+}Ti_4O_{12}$. The $CaCu_3Ti_4O_{12}$ is used as a pure divalent reference for the A'-site Cu ion with a CuO_4 square-planar coordination, which has the same local environment as CCCIO for Cu ions at the A' site. One can see a sharp peak at the Cu–L_3 edge in $CaCu_3Ti_4O_{12}$ and CCCIO owing to the dipole transition $2p^63d^9 \rightarrow 2p^53d^{10}$,[21] reflecting the same Cu^{2+} valence state. However, there is an energy shift about 0.29-eV higher from $CaCu_3Ti_4O_{12}$ (931.37 eV) to CCCIO (931.66 eV). That can be understood by the different local environment of Cu. The Cu^{2+} ions in CCCIO have square-planar coordination and octahedral coordination at the same time. The $Ca_{0.83}CuO_2$ is adopted as another reference with mixed Cu^{2+} and Cu^{3+} states.[22] The energy position of the Cu^{2+} related peak in the mixed-valence $Ca_{0.83}CuO_2$ shifts by about 0.25 eV toward the higher energy side relative to $CaCu_3Ti_4O_{12}$. Because the Cu ions in $Ca_{0.83}CuO_2$ and $CaCu_3Ti_4O_{12}$ have a similar local square-planar coordination, but the Cu–O network in the former is edge-shared, whereas the CuO_4 units in $CaCu_3Ti_4O_{12}$ are separated from each other. For $Ca_{0.83}CuO_2$, the sharp Cu^{3+}-related peak at 933.57 eV in Fig. 3(a) is assigned to $3d^9\underline{L}$, where $\underline{L}$ stands for hole at O-2p states. It is only observed for an edge-shared or an isolated Cu–O network,[23,24] while the Cu^{3+}ion-related spectral feature with a corner-shared Cu–O network shows only a broad shoulder above the Cu^{2+}-related peak.[25,26] Thus, we can conclude that our sample is free from Cu^{3+} ions: all the Cu ions in CCCIO are Cu^{2+} states.

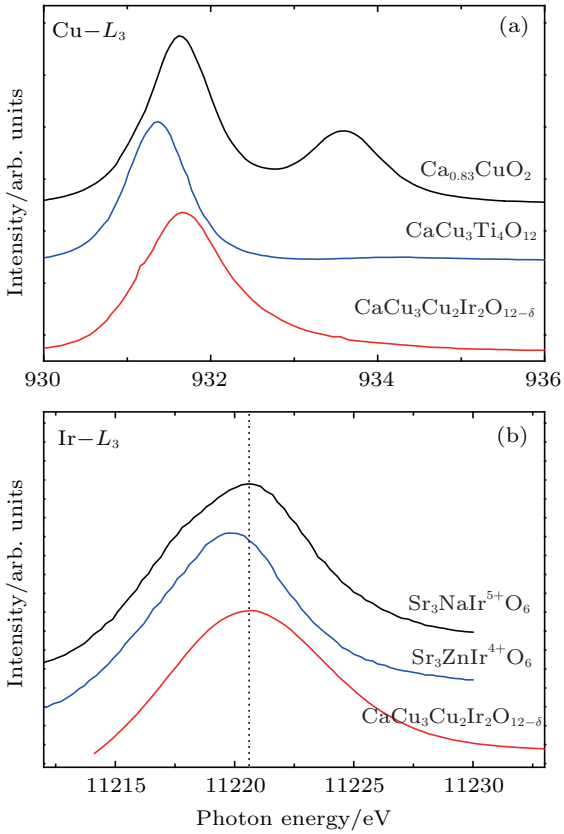


Fig. 3. (color online) XAS of (a) Cu–L_3 edge, (b) Ir–L_3 edge of $CaCu_3Cu_2Ir_2O_{12-\delta}$. The XAS spectra of some related references are also shown for comparison.

The XAS of CCCIO along with $Sr_3ZnIr^{4+}O_6$ and $Sr_3NaIr^{5+}O_6$ are shown in Fig. 3(b). These two references with different Ir valence states have the same local environment (IrO_6 octahedra).[27] By comparison, the white line in the Ir–L_3 edge of CCCIO lies at the same energy position as that of Sr_3NaIrO_6 with Ir^{5+}, and deviates from $Sr_3ZnIr^{4+}O_6$. As a result, XAS measurements prove the presence of Ir^{5+} in CCCIO. Having determined the A'-site Cu^{2+}, the B-site Cu^{2+} valence states and the B-site Ir^{5+} valence states, we conclude that CCCIO is nonstoichiometric, in connection with the slight oxygen deficiency.

The magnetic susceptibility of CCCIO as a function of temperature is shown in Fig. 4(a). With temperature decreasing down to 2 K, no long-range magnetic phase transition is observed. Above 100 K, the susceptibility is nearly temperature-independent, probably suggesting metallic Pauli paramagnetic behavior. The Curie-like upturns observed at low temperatures may originate from a small amount of impurity phases, which are undetectable by XRD.[28] Figure 4(b) shows the field dependence of isothermal magnetization measured at different temperatures. The linear magnetization behaviors are consistent with the paramagnetic feature as deter-

mined from the magnetic susceptibility measurements.

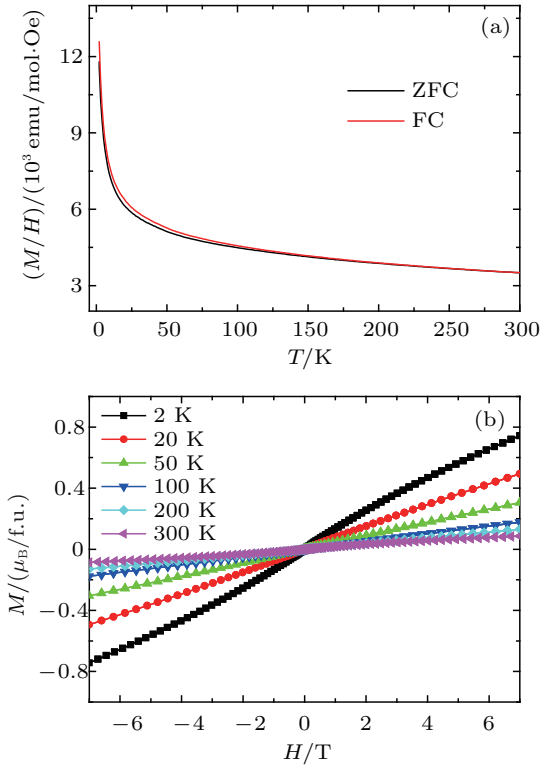


Fig. 4. (color online) (a) Temperature dependence of magnetic susceptibility of $CaCu_3Cu_2Ir_2O_{12-\delta}$ measured at zero-field cooling (ZFC) and field cooling (FC) modes with applied field 0.1 T. (b) Field dependence of the magnetization at different temperatures. The unit 1 Oe = 79.5775 A·m^{-1}.

As is well known, the Ir^{5+} ions ($5d^4$) has a $J_{\mathrm{eff}} = 0$ singlet ground state in the strong spin–orbit coupling limit.[29] This means that the *B*-site Ir^{5+} in the present CCCIO is nonmagnetic in nature. Although it is possible for the *B*-site Cu^{2+} ($3d^9$) to take part in spin ordering as observed in Sr_2CuIrO_6,[30] the random distribution between Cu^{2+} ions and the nonmagnetic Ir^{5+} is unfavorable for the formation of long-range magnetic ordering at the *B* site in CCCIO. In addition, in $CaCu_3Ge_4O_{12}$ and $CaCu_3Sn_4O_{12}$, the *A*′-site Cu^{2+} ions can induce a ferromagnetic phase transition via the Cu–Cu direct interactions. On the other hand, in $CaCu_3Ti_4O_{12}$, the d^0-orbits of Ti^{4+} ions are found to contribute to the antiferromagnetic ordering through the Cu^{2+}–O–Ti^{4+}–O–Cu^{2+} super-superexchange pathway.[31–34] In our CCCIO, since the d-orbits of the *B*-site transition metals are disordered, no long-range spin ordering can be formed in the whole temperature range we measured (2 K–300 K).

Figure 5 shows the temperature dependence of resistivity for CCCIO. With decreasing temperature, the resistivity increases slightly from 14 mΩ·cm at 300 K to 24 mΩ·cm at 2 K. As shown in Fig. 1, the $A'O_4$ units in the *A*-site ordered perovskite are separated from each other in space, the electrical transport therefore should be dominated by the corner-sharing BO_6 octahedra. Considering that the resistivity of CCCIO is measured on a polycrystalline pellet, where the grain-boundary scattering plays an important role,[35] the observed small, and only slightly temperature-dependent, resistivity values may imply the delocalized electronic feature for the *B*-site disordered Ir^{5+} and Cu^{2+} ions. Actually, in $Sr_2Fe_{1-x}Cu_xMoO_6$ with Cu^{2+} ions, and in $Ba_{0.5}IrO_3$ with Ir^{5+} ions, metallic electrical conductivities were observed.[36,37] The resistivity data of CCCIO in 270 K–300 K can be well fitted by using the thermal activation model with the formula $\rho = \rho_0\, e^{E_A/KT}$ as shown in the inset of Fig. 5. Here E_A and K stand for thermal activation energy and the Boltzmann constant, respectively. The fitting gives $E_A = 3.05(2)$ meV. This very small and probably physically meaningless activation energy may also reflect the delocalized behavior of the polycrystalline CCCIO.

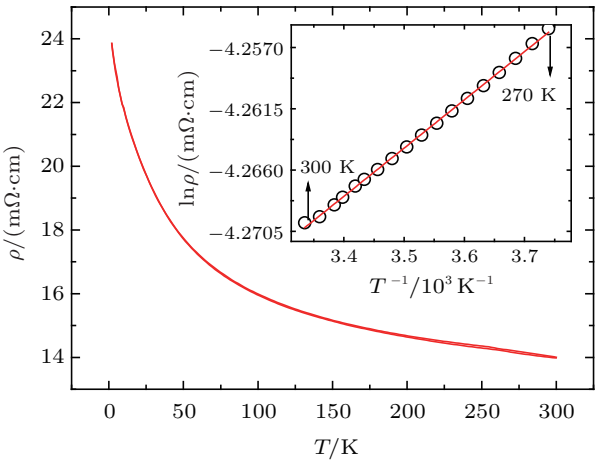


Fig. 5. (color online) Temperature dependence of resistivity of $CaCu_3Cu_2Ir_2O_{12-\delta}$. The inset shows the fitting result using the thermal activation model. The open circles represent experimental data, and the red line is the fitting result.

To further understand the transport properties of CCCIO, heat capacity (C_P) was measured as shown in Fig. 6. In the temperature region we measured (2 K–200 K), we do not find any anomaly in C_P, in agreement with the absence of any long-range spin ordering. The inset of Fig. 6 presents the low-temperature fitting result using the formula $C_P/T = \gamma + \beta T^2$, where the γT and βT^3 terms describe the electron and lattice contributions to the total heat capacity, respectively. The obtained coefficient γ is equal to 0.211(8) J·mol^{-1}·K^{-2}, which is larger than that of β (0.0039(3) J·mol^{-1}·K^{-4}) by two orders of magnitude. Therefore, the electron contribution dominates the low-temperature heat capacity, confirming the intrinsic itinerant electronic behavior of CCCIO, related to the *B*-site-disordered Cu^{2+} and Ir^{5+} ions.

In order to investigate structural stability of CCCIO under high pressure, the SXRD was carried out at room temperature. Figure 7(a) shows some representative SXRD patterns collected at different pressures. As the pressure increases, one can find that all the diffraction peaks systematically shift towards higher 2θ values as expected from the unit cell volume contraction. No visible structural phase transition is observed

in the pressure region we applied, suggesting that the crystal structure of CCCIO is stable up to 35.7 GPa. Figure 7(b) shows the related pressure dependence of lattice constant. It monotonously decreases with increasing pressure without any profound change.

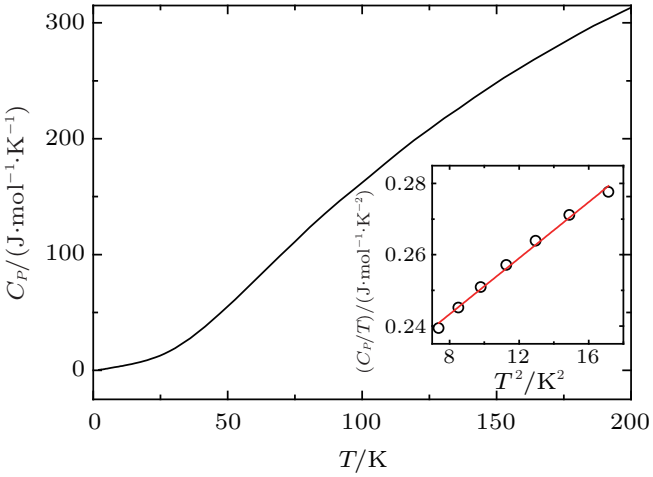


Fig. 6. (color online) Heat capacity as a function of temperature for $CaCu_3Cu_2Ir_2O_{12-\delta}$. The inset shows the fitting result described in the text. The open circles represent experimental data, and the red curve is the fitting result.

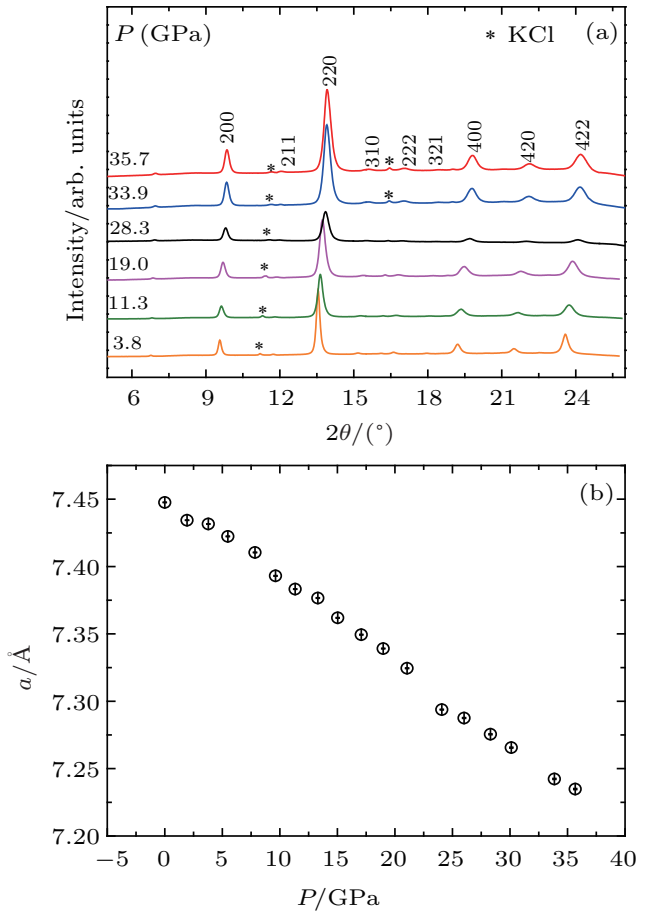


Fig. 7. (color online) (a) SXRD patterns of $CaCu_3Cu_2Ir_2O_{12-\delta}$ at selected pressures and room temperature. The asterisks stand for the diffraction peak originating from KCl impurity phase. (b) Pressure dependence of lattice constant of $CaCu_3Cu_2Ir_2O_{12-\delta}$. The error bars are located within the data symbols.

4. Summary

In summary, polycrystalline $CaCu_3Cu_2Ir_2O_{12-\delta}$ has been prepared for the first time, by a high-pressure, high-temperature method. The Rietveld refinement reveals that this compound crystallizes in an *A*-site ordered but *B*-site disordered perovskite structure with space group *Im*-3. Both BVS calculation and XAS confirm the charge states to be Cu^{2+} and Ir^{5+}. Because of the disordered distribution of the *B*-site Ir^{5+} and Cu^{2+}, no long-range magnetic phase transition is observed in the whole temperature region we measured (2 K–300 K). The susceptibility approximately shows a temperature-independent Pauli paramagnetic behavior. Based on the analysis of resistivity data, we infer delocalized electrical behavior for the present CCCIO. Furthermore, the itinerant electronic feature is confirmed by heat capacity analysis, with the electron contribution dominating the low-temperature heat capacity. High-pressure SXRD measurement does not show any evidence for possible structural phase transition, revealing the structural stability of CCCIO with pressure up to 35.7 GPa at room temperature.

References

[1] Shiraki H, Saito T, Yamada T, Tsujimoto M, Azuma M, Kurata H, Isoda S, Takano M and Shimakawa Y 2007 *Phys. Rev. B* **76** 140403(R)
[2] Kayser P, Retuerto M, Sanchez-Benıtez J, Martínez-Lope M J, Fernández-Díaz M T and Alonso J A 2012 *J. Phys.: Condens. Matter* **24** 496002
[3] Shimakawa Y and Saito T 2012 *Phys. Status Solidi B* **249** 423
[4] Koitzsch A, Blumberg G, Gozar A, Dennis B, Ramirez A P, Trebst S, and Wakimoto S 2002 *Phys. Rev. B* **65** 052406
[5] Long Y W, Hayashi N, Saito T, Azuma M, Muranaka S and Shimakawa Y 2009 *Nature* **458** 07816
[6] Long Y W, Saito T, Tohyama T, Oka K, Azuma M and Shimakawa Y 2009 *Inorg. Chem.* **48** 8489
[7] Long Y W and Shimakawa Y 2010 *New J. Phys.* **12** 063029
[8] Hao X F, Xu Y H, Gao F M, Zhou D F and Meng J 2009 *Phys. Rev. B* **79** 113101
[9] Yamada I, Tsuchida K, Ohgushi K, Hayashi N, Kim J, Tsuji N, Takahashi R, Matsushita M, Nishiyama N, Inoue T, Irifune T, Kato K, Takata M and Takano M 2011 *Angew. Chem. Int. Ed.* **50** 6579
[10] Cai L G, Liu F M and Zhong W W 2010 *Chin. Phys. B* **19** 097101
[11] Han D D, Gao W, Li N N, Tang R L, Li H, Ma Y M, Cui Q L, Zhu P W and Wang X 2013 *Chin. Phys. B* **22** 059101
[12] Fang Y, Yan S M, Qiao W, Wang W, Wang D H and Du Y W 2014 *Chin. Phys. B* **23** 117501
[13] Subramanian M A, Li D, Duan N, Reisner B A and Sleight A W 2000 *J. Solid State Chem.* **151** 323
[14] Larson A C and Von Dreele R B 2004 *General Structure Analysis System (GSAS)*, Los Alamos National Laboratory Report No. LAUR 86-748.
[15] Mao H K, Xu J and Bell P M 1986 *J. Geophys. Res.* **91** 4673
[16] Byeon S H, Lee S S, Parise J B, Woodward P M and Hur N H 2004 *Chem. Mater.* **16** 3697
[17] Byeon S H, Lee S S, Parise J B, Woodward P M and Hur N H 2005 *Chem. Mater.* **17** 3552
[18] Byeon S H, Lee S S, PariseJ B and Woodward P M 2006 *Chem. Mater.* **18** 3873
[19] Anderson M T, Greenwood K B, Taylor G A and Poeppelmeiert K R 1993 *Prog. Solid State. Chem.* **22** 197
[20] Cheng J G, Zhou J S, Yang Y F, Zhou H D, Matsubayashi K, Uwatoko Y, MacDonald A and Goodenough J B 2013 *Phys. Rev. Lett.* **111** 176403
[21] Salluzzo M, Ghiringhelli G, Brookes N B, De Luca G M, Fracassi F and Vaglio R 2007 *Physica C* **460** 971

[22] Huang M J, Deng G, Chin Y Y, Hu Z, Cheng J G, Chou F C, Conder K, Zhou J S, Pi T W, Goodenough J B, Lin H J and Chen C T 2013 *Phys. Rev. B* **88** 014520
[23] Hu Z, Drechsler S L, Malek J, Rosner H, Neudert R, Knupfer M, Golden M S, Fink J, Karpinski J and Kaindl G 2002 *Europhys. Lett.* **59** 135
[24] Hu Z, Mazumdar Chandan, Kaindl G, de Groot F M F, Warda S A and Reinen D 1998 *Chem. Phys. Lett.* **297** 321
[25] Chen C T, Tjeng L H, Kwo J, Kao H L, Rudolf P, Sette F and Fleming R M 1992 *Phys. Rev. Lett.* **68** 2543
[26] Meyers D, Mukherjee Swarnakamal, Cheng J G, Middey S, Zhou J S, Goodenough J B, Gray B A, Freeland J W, Saha-Dasgupta T and Chakhalian J 2013 *Sci. Rep.* **3** 1834
[27] Mugavero III S J, Smith M D, Yoon W S and Loye H Z 2009 *Angew. Chem. Int. Ed.* **48** 215
[28] Shimakawa Y 2008 *Inorg. Chem.* **47** 8562
[29] Cao G, Qi T F, Li L, Terzic J S, Yuan J, DeLong L E, Murthy G and Kaul R K 2014 *Phys. Rev. Lett.* **112** 056402
[30] Vasala S, Yamauchi H and Karppinen M 2014 *J. Solid State Chem.* **220** 28
[31] Mizumaki M, Saito T, Shiraki H and Shimakawa Y 2009 *Inorg. Chem.* **48** 3499
[32] Krohns S, Lu J, Lunkenheimer P, Brize V, Autret-Lambert C, Gervais M, Gervais F, Bouree F, Porcher F and Loidl 2009 *Eur. Phys. J. B* **72** 173
[33] Shimakawa Y, Shiraki H and Saito T 2008 *J. Phys. Soc. Jpn.* **77** 113702
[34] Kim Y J, Wakimoto S, Shapiro S M, Gehring P M and Ramirez A P 2002 *Solid State Commun.* **121** 625
[35] Paul A K, Jansen M, Yan B H, Felser C, Reehuis M and Abdala P M 2013 *Inorg. Chem.* **52** 6713
[36] Yuan C L, Zhu Y and Ong P P 2002 *J. Appl. Phys.* **91** 4421
[37] Sleight A W 1974 *Mater. Res. Bull.* **9** 1177